Numerical study of fully baffled super-X L-mode discharges on TCV

C. Meineri[a,*], P. Muscente[b], C. Theiler[c], D. Galassi[c], TCV team[1], and the MST1 team[2]

[a]NEMO Group, Dipartimento Energia, Politecnico di Torino, Corso Duca degli Abruzzi 24, 10129, Torino, Italy
[b]Centro di Ateneo "Centro Ricerca e fusione" c/o Consorzio RFX, Padova University, Italy
[c]Ecole Polytechnique Fédérale de Lausanne (EPFL), Swiss Plasma Center (SPC), CH-1015 Lausanne, Switzerland

Abstract

We present a numerical study of three fully baffled L-mode TCV discharges with three different values of the outer strike-point major radius/total flux expansion, showing that the beneficial effect of large strike point radius is partially screened in these experiments by a not perfectly equalised neutral divertor trapping. The assessment of the SOL and divertor plasma conditions is made with the SOLEDGE2D-EIRENE plasma edge code. The simulation results show that artificially increasing the outer baffle length induces a 30% decrease in the neutral particles influx at the last closed surface LCFS and main SOL plasma in scenarios with large strike point radius. This causes a drastic reduction of plasma temperature on the divertor target in these cases, approaching the two point model (TPM) expectation. Instead a longer outer baffle is predicted to be negligible for the smallest strike point radius, where the neutrals are already well confined with the actual geometry of the baffle. This numerical work illustrated the different challenges to face during the experiments to retrive the full benefits expected from total flux expansion, most of it related to geometry and magnetic wall allinement, giving some hints to reduce the difference between the ideal experiment and the real one.

Keywords: SOLEDGE2D-EIRENE, Tokamak TCV, Super-X

1. Introduction

One of the main problems facing future fusion reactors, (such as DEMO [1]), is the heat flux deposited on the first wall and in particular on the divertor plates, where most of the power load typically arrives. Without radiation produced by extrinsic impurities or other radiative mechanisms, the predicted peak power load on the target plate materials will greatly exceed the $\sim 10 MW/m^2$ maximum limit of current plasma-facing component technology. The detachment regime [7] is characterized by a large reduction of plasma particle flux and heat load on the divertor plate and it's important to achieve for future fusion reactors. Alternative divertor magnetic configurations are a potentially promising means for reducing the plasma and impurity density thresholds for detachment and/or provide passive stabilization of the detachment front. One of this particular configurations is the Super-X [4], which shows theoretically the anticipation of detachment onset as the outer divertor separatrix leg position and the strike-point major radius, R_t, are increased. The different experiments on DIII-D [4] and the initial TCV experiments [8] without baffles don't illustrated a complete agreement with the expected trend. One plausible reason is the different neutral confinement in the different Rt cases related to geometry design characteristics and the strike-point angle, as shown by the SOLPS modeling [9]. It has been demonstrated that in order to have more similar divertor neutral confinement, it is necessary to force a constant angle beta in the simulations (the poloidal incidence angle between divertor leg and wall) as well as add very strong baffling. Based on these predictions, more optimised experiments have been performed [2]. However, they still showed considerable deviations from the simple TPM. This work presents the SOLEDGE2D-EIRENE simulation results of three fully baffled super-X L-mode discharges on the *Tokamak á Configuration Variable* (TCV) [6] at three different values of the total flux expansion $f_t = \frac{B_{tot,u}}{B_{tot,t}}$, where B_{tot} is the norm of the magnetic field, u indicates the equatorial (upstream) plane and t the position of the separatrix strike point on the divertor targets. The divertor leg has been scanned in the experiments, shifting the outer strike point to three different values of the major radius R_t (0.62 m, 1.01 m, and 1.08 m) with consequent lowering of the total field at the strike-point. The reduction of the detachment threshold during the experimental discharges is less than half of what is predicted by the previous modelling [2] and by the modified version of the TPM [4]. After a brief description in section two of experimental pulses and modeling set-up, in the third section of the paper we illustrate the simulation results for the three different scenarios imposing the same transport coefficients and physical parameters. The simulations show a discrepancy with respect to the simple TPM, while they have qualitatively a similar behaviour as the experiments. In the fourth section, The actual outer baffle is substituted with a longer baffle length to reduce the number of neutral particles escaping from the divertor region and its effects on target profiles and detachment threshold in the three different scenarios is studied.

*Corresponding author
Email address: carlo.meineri@polito.it (C. Meineri)
[1]See author list of H. Reimerdes et al 2022 Nucl. Fusion 62 042018
[2]see author list of B. Labit et al 2019 Nucl. Fusion 59, 086020

2. Comparison set-up and modeling strategy

The three experimental cases compared are L-mode plasma discharges with an Ohmic heating power $P_{ohm} \approx 280kW$ and a plasma current of $I_p = 250kA$, fig. 1. The three cases are characterized by a density ramp during the flattop, necessary to evaluate the detachment onset via the C_{III} carbon radiation [2]. The pulse #70202 has the outer strike point at $R_t = 0.62m$ on the HFS vertical wall, fig. 2 (B) color blue, the #70201 at $R_t = 1.01m$ on the outer part of the wall, magenta line, and the #70207 at $R_t = 1.07m$, red line on the LFS wall. The small and the large R_t cases have similar poloidal flux expansion $f_t = 2.5 - 2.9$ and similar poloidal incidence angle $\beta = 114° - 111°$. For technical reasons, the extreme R_t scenario could not achieved such properties having $f_t = 1.4$ and $\beta = 80°$.

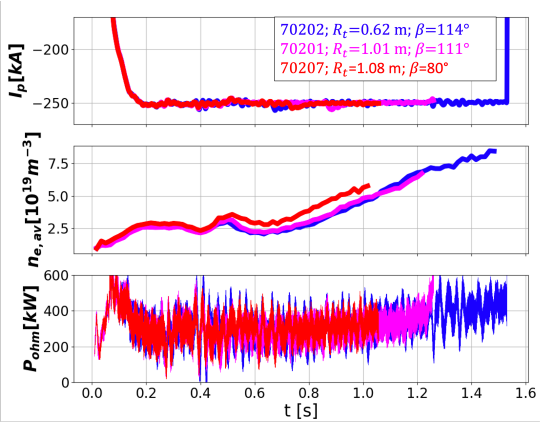

Figure 1: Plasma current (I_p), average electron density ($< n_e >$) and ohmic heating P_{ohm} as a function of time of the three L-mode scenarios studied in this work.

These three cases have been modelled with SOLEDGE2D-EIRENE [10], which is a 2D multi-fluid code solving Braginskii equations, with a diffusive ansatz on cross-field transport. Being coupled with EIRENE, it also includes plasma-neutrals interactions. One of this code's main distinguishing features is the extension of the computational mesh up to the first wall, that enables to measure the power flux over all the surfaces, by means of a numerical technique called "penalisation". The radial profile of the transport coefficients D and $\chi_{i,e}$ (m^2s^{-1}), fig. 3, describing respectively the particle and the energy transport along the radial direction, have chosen to get a reasonable agreement between simulation results and upstream and downstream experimental data from Thomson Scattering (TS), fig. 2 (C), Langmuir Probes (LP) and Bolometry (BOLO), fig. 2 (C). The same input parameters and same transport coefficients are applied at all three cases in order to inspect the effect of the total flux expansion independently from possibly different cross-field transport properties. Carbon impurites are introduced via physical and chemical sputtering on all plasma-facing components (PFCs). Physical sputtering follows the Roth-Bohdanky formula [**?**] and it is typically small w.r.t chemical sputtering, where a yield of 3.5% is assumed. The carbon recycling coefficient, being challenging to determine in experiments, is imposed to be $r_C =$

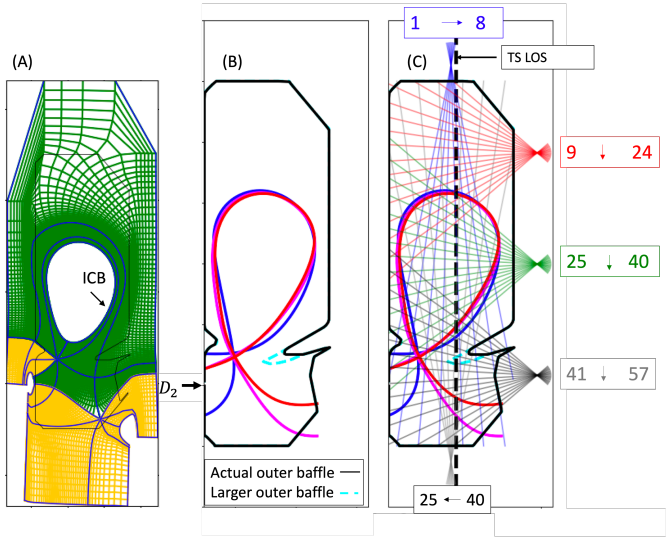

Figure 2: (A) Example of SOLEDGE2D mesh for #70202 where the inner core boundary ICB is indicated, (B) TCV poloidal cross section showing the separatrix of the three cases, the actual outer baffle (black) and the new one (cyan); (C) Line of sight of TS and BOLO; the small R_t case is in blue, the large R_t case in magenta and in red the extreme R_t;

0.73 on carbon tiles in order to obtain a total radiated power in the SOL in agreement with the bolometry experimental data. For the Deuterium the recycling coefficient has been assumed $r_D = 0.99$. The heating power crossing the radially inner core boundary is distributed equally between electrons and ions and chosen to match the power crossing the separatrix for all the three cases. The gas puff has been adjusted in each geometry to have the same electron density at the separatrix $n_{e,sep}$ for the three cases. Deuterium molecules are puffed from the PFR region, fig. 2 (B), and the particle flux over the core boundary is set to zero, fig. 2 (A). The drifts and neutral-neutral interactions are not taken into account in this work.

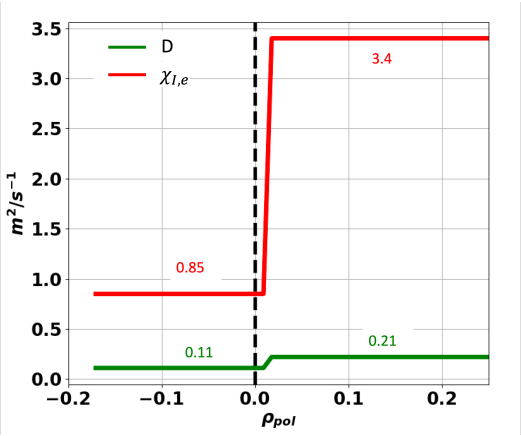

Figure 3: Transport coefficients for particle D and energy $\chi_{e,i}$;

3. Simulation results with the actual outer baffle

3.1. Upstream plasma parameters and profiles

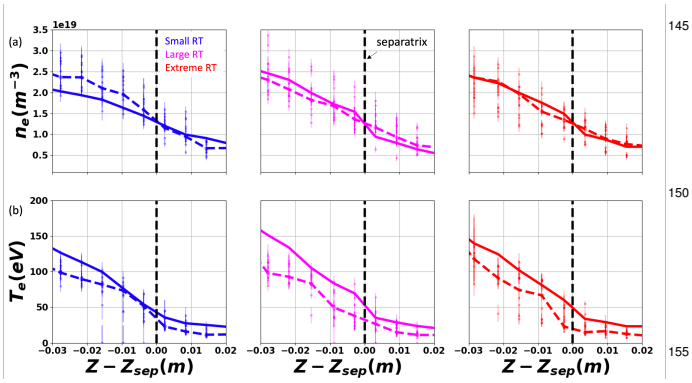

Figure 4: SOLEDGE2D electron density n_e and temperature T_e along the LOS of TS, where the blue solid line represents the small, the magenta the large and the red the extreme R_t cases. The dots are the experimental data, with their error-bar. The dashed line is the average value in the time interval.

The electron density n_e and temperature T_e along the TS LOS are shown respectively in fig. 4 (a) and (b), where the solid lines represent the SOLEDGE2D results and the dots are the experimental data. The time interval chosen is 100 ms around the time when the average density value at the separatrix is $< n_{e,sep} >= 1.3e19m^{-3}$ and the dashed line is the average of experimental data. The experimental and simulated n_e profiles agree within error bars for the large and extreme R_t cases but the agreement is less good for the small R_t case, where the simulated profile is flatter than the experimental one, resulting in a density inside the core $n_{e,core} \approx 20\%$ lower (dashed blue line) and a SOL density $n_{e,sol} \sim 30\%$ higher than in the experiments. This difference is related to the better neutral divertor confinement in the small R_t and his effect is consistent with the previous SOLEDGE2D simulations [5], where the baffle closure scan has a direct impact on the neutral compression. This factor can be define as the ratio between the average total neutral density in the divertor and in the main chamber, $c_D = \langle n_n \rangle_{div} / \langle n_n \rangle_{main}$. Similar to [5] the divertor and main chamber zone are divided by line that connect the two baffles, passing under the x-point. The $c_D \approx 65$ in the small R_t case, $c_D \approx 30$ in the large R_t case and $c_D \approx 55$ in the extreme R_t case. This result can be affected by the line position because the rapid drop of neutrals at the X-point height but different small variations seems weakly affected the c_D. The large R_t has the lowest puffing, $3.01 * 10^{20} part/s$ and the small R_t has a puffing of $4.5 * 10^{20} part/s$ not so different from extreme R_t, $3.97 * 10^{20} part/s$. If the beneficial effect of super-X in large R_t is probably screened by a low neutral confinement, in the case of extreme R_t could be a mix of neutral confinement and the different *beta* angle to the wall with large and small R_t. This last feature will be investigated in a separate work in the future. For all the cases the electron temperature is larger than the average value but inside the error bar. This over-estimation is necessary to have a better agreement with the experimental data on the outer target. This over-estimation of the electron temperature at the target is common for 2D transport codes as SOLEDGE2D and SOLPS-ITER [11].

3.2. SOL radiation and comparison with bolometry

The total input power $P_{input} = P_{ohm} - P_{rad,core}$ of the simulation is the ohmic power ($\approx$ 280 kW) , from which we substract the total radiation from the portion of the core not included in SOLEDGE2D mesh ($\sim 15kW$). This information has been extracted from the tomographic inversion of the radiation measured by the bolometry. The carbon recycling coefficient $r_C = 0.73$ has been set for all the three cases to obtain a simulated total radiation of $P_{rad} \sim 100kW$ as observed from the Bolometer's data. The radiation distribution in the SOL can be investigated with the synthetic bolometers, developed for TCV SOLEDGE2D simulations, which allow a direct comparison with the calibrated bolometric chord brightness $[W/m^2]$. The comparison between experimental and simulated brightness values at all the available LOS is exposed in fig. 5. The dashed black vertical line indicated the position of the inner and outer target. The small R_t case, fig. 5 (A), has the best agreement with the bolometry LOS, expecially near the outer target. There is a lack of information for the inner target, where working LOS data are not present. The large and extreme R_t show a less good agreement, in particular on the targets (orange shaded area) where the simulated chord brightness exceeds the measured values. We obtain a reasonable agreement in the rest of the domain, for the three cases. The SOLEDGE2D radiation is more concentrated at the strike points, instead the tomographic reconstruction of the measurements shows an high radiation zone around the x-point. It is not clear whether the divertor carbon content is overestimated or the plasma conditions are more favorable to promoting carbon radiation.

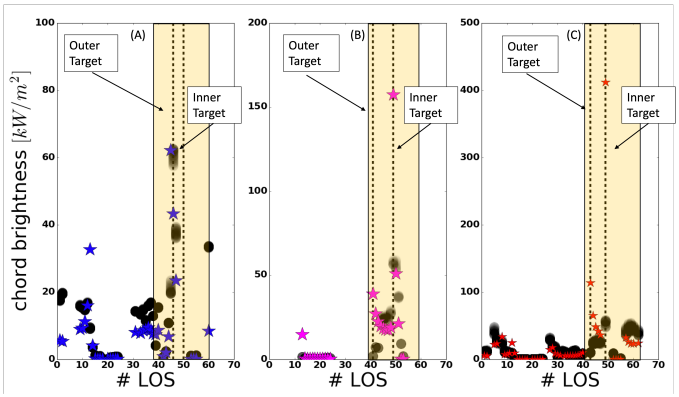

Figure 5: BOLO LOS for the small (A), large (B) and extreme (C) R_t. The stars represent the simulation results and the black dot the experimental data

3.3. Target plasma parameters and profiles

All the three cases, fig. 6, have an over-estimation of density $n_{e,t}$ peak with respect to experiments (a factor 3 for small, factor 2 for the large and extreme case), whereas J_{sat}, fig. 7 (c), shows a better agreement with the experimental data (the peak is overestimated by a factor $\sim$ 1.2). The electron temperature

$T_{e,t}$ peak, fig. 7 (b), is in agreement in the small and extreme R_t case, while it is underestimated in the large R_t case. As we will explain in the previous paragraph, there is high uncertainty on carbon wall emission and its radiation, which could be the cause of these discrepancies. In particular the large R_t case shows a $T_{e,t}$ peak lower than the extreme R_t, contrarily to what we expected from the experimental data. This difference could be related to the β angle at the wall that could also affect carbon sputtering emission. This point will be studied in the near future with dedicated simulations, trying to find a way to fix the same β for all three cases. The large and extreme R_t deviates from the TPM in both experimental and simulated data,dashed black line in fig. 6 and fig. 7, with lower density and higher temperature than expected scaling. As we will show in the next chapter, this is in part related to the neutral confinement and better results can be obtained with a longer outer baffle. The small R_t case simulation result has been used as reference to calculated the expected TPM profiles for larger and extreme R_t.

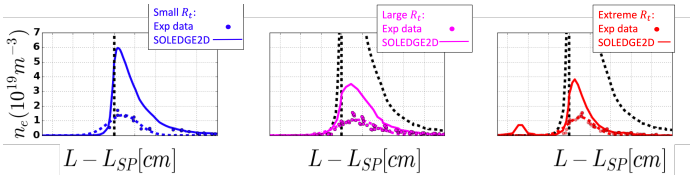

Figure 6: Zoom of Outer-target electron density n_e comparison between experimental data and SOLEDGE2D. For more detail see the legend in fig. 7

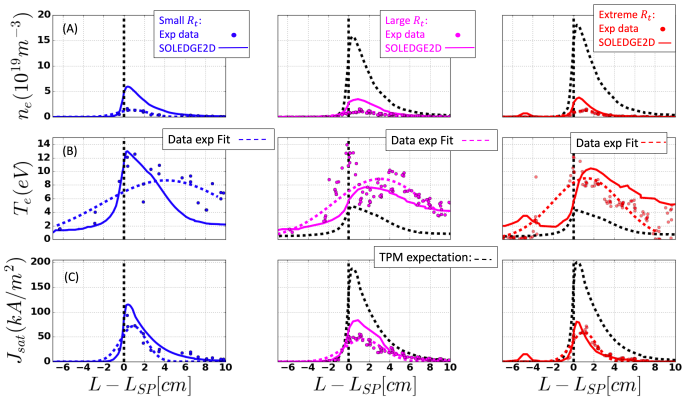

Figure 7: Outer-target electron density n_e,temperature T_e and ion saturation current J_{sat} comparison between experimental data and SOLEDGE2D. The coordinate on the abscissa is along the wall and the dashed black line represents the position of the strike-point. In the first column is displayed the small R_t case, where the experimental data are drawn as blue dots and the dashed blue curve is the fit of the data. In the second and third column are shown the large and extreme R_t, respectively in magenta and red. The black dashed curve are the expected simple TPM results $T_{(e,t)} \propto \frac{1}{(R_t^2)}$; $n_{(e,t)} \propto R_t^2$, $J_{sat} \propto R_t$ for large and extreme R_t.

4. Effect of a longer outer-baffle

In the simulations that we have discussed until now, featuring the actual geometry of the outer baffle in TCV, the small R_t case has the neutral compression factor higher than the other two cases because the neutrals n_D are better confined in the divertor region than the main chamber. We now consider a baffle with an additional extension inside the machine of 9 cm, the different between the length of the two baffles, as shown in fig. 2 B.

The *longer outer baffle* reduces by $\sim$ 30% the total n_D at the LCSF in large R_t, fig. 8, and of $\sim$ 10% for the extreme R_t, fig. 9, having a large impact on the outer target results and on the total radiation. In both fig. 8 and fig. 9, the neutral particles coming from the outer leg and entering the core through the LCFS are greatly reduced and the peak at 270° on the LCFS for large and extreme R_t disappear introducing the longer outer baffle. Only the neutral particle flux from the inner leg at 250° on the LCFS remain because not affected by the outer baffle but the inner one. The compression factor became $c_D \approx 75$ in the small R_t case, $c_D \approx 162$ in the large R_t case and $c_D \approx 200$ in the extreme R_t case. The small R_t has negligible effect instead the other two increase their compression factor higher then the small case, with a similar neutral density on the LCFS to the small case.

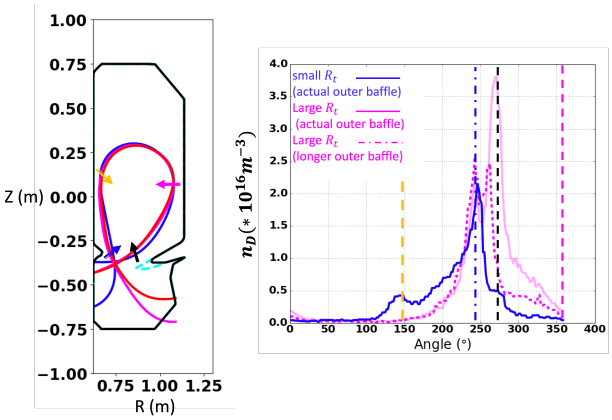

Figure 8: Neutral deuterium density (B) n_D along the LCFS as a function of the poloidal angle. The peak at 150° (orange dashed line in figure (B) and orange arrow in figure (A)) is the inner mid-plane at HFS, the peak at 250° (blue dashed line in figure (B) and blue arrow in figure (A)) is inner baffle at HFS near the equatorial plane, the peak at 270° (dashed black line in figure (B) and black arrow in figure (A)) is outer baffle at HFS. The outer mid-plane is at 360° and 0°. The small R_t case, blue line, is compared with the large R_t with the actual outer baffle, magenta continuous line, and with the longer outer baffle results, magenta dashed line.

The J_{sat} peak, when increasing the baffle length, increases, fig. 10, by 50% in large R_t and 25% in the extreme R_t but it is still less than the simple TPM expectation, fig. 7 . Instead $T_{e,t}$ has a drastic drop for the large and extreme R_t (negligible effect for the small one), with temperatures around $\sim 3eV$, similar to what we expected with the TPM.

These differences could be globally related to the power, momentum loss and the carbon radiative efficiency as function of T_e [3] inside the simulation. As is possible to see in fig. 11 and fig. 12 for the large and extreme R_t, the total Deuterium and Carbon density increases in the divertor region below the longer outer-baffle, in particular in the far SOL covered by the longer outer baffle. This is caused by the increasing of compression factor for both species. The total power loss in the divertor

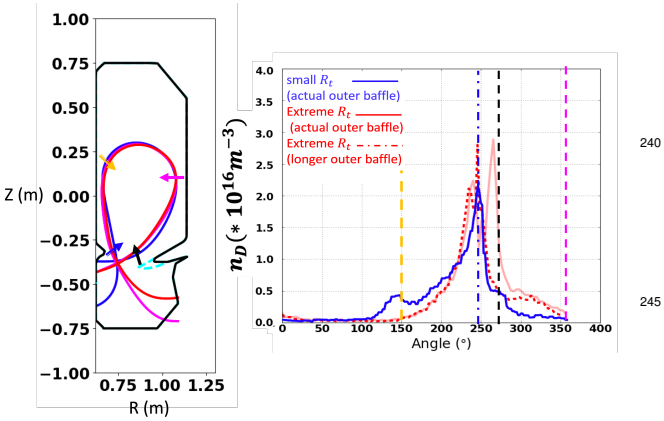

Figure 9: Neutral deuterium density (B) n_D along the LCFS as a function of the poloidal angle. The peak at 150° (orange dashed line in figure (B) and orange arrow in figure (A)) is the inner mid-plane at HFS, the peak at 250° (blue dashed line in figure (B) and blue arrow in figure (A)) is inner baffle at HFS near the equatorial plane, the peak at 270° (dashed black line in figure (B) and black arrow in figure (A)) is outer baffle at HFS. The small R_t case, blue line, is compared with the extreme R_t with the actual outer baffle, red continuous line, and with the longer outer baffle results, red dashed line.

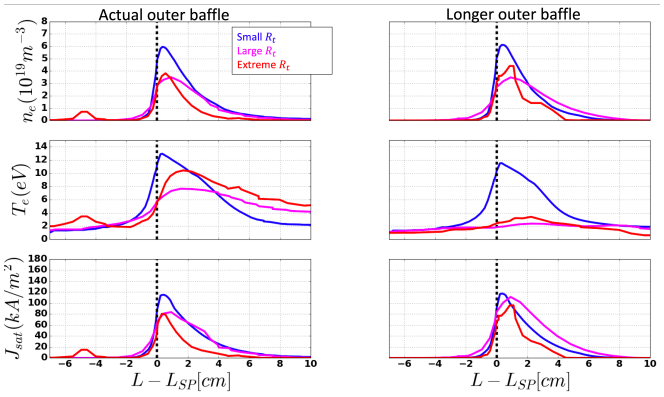

Figure 10: Outer-target electron density $n_{e,target}$,temperature $T_{e,target}$ and particle flux j_{sat} comparison between actual outer baffle (left column) and longer outer baffle (right column). The coordinate is along the wall and the dashed black line is the position of the strike-point. The expected simple TPM is in black dashed line.

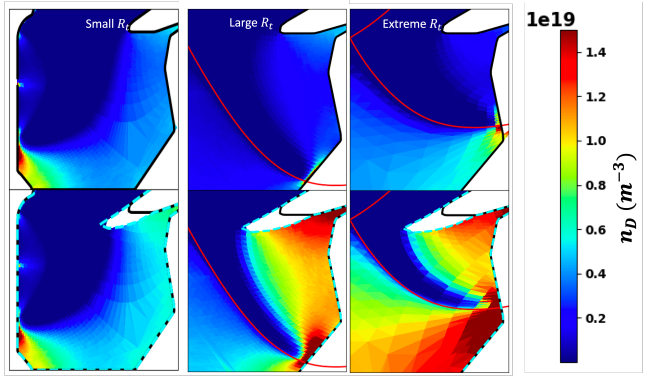

Figure 11: 2D divertor color plot of total neutral density D with the actual outer baffle (top row) and longer outer baffle (lower row). For the large and extreme R_t there is shown only the outer leg and strike point, where most the changes appear.

region through radiation grows and the peak of the ionization is reduced in front of the wall, fig. 13. Increasing the compression factor, the neutral particles are more trapped by the baffling, and the higher neutral pressure enhances plasma–neutral collisions. The latter increases the radiative and charge exchange (CX) losses, leading to a reduction of T_e. The radiative efficiency of carbon increases inversely proportional to the electron temperature with the maximum at $\sim 3eV$. Therefore the power load on the outer target is reduced with the longer outer baffle by $\sim 25\%$ and $\sim 30\%$ for large and extreme R_t, where $\sim 80\%$ of the reduction is caused by Carbon and deuterium radiation. The other 20% of the reduction is because of the power that is is intercepted by the longer outer baffle. This longer baffle impacts marginally the small R_t case, with a small increase of carbon density and radiation in the far SOL and the peak of ionization remains in front of the target. The momentum source, the neutral plasma-interactions acting of momentum sink with charge-exchange, fig. 14 increases for the large and extreme R_t with the longer outer baffle. The consequent pressure drop can be define as $p_{drop} = p_{tot,t}/p_{tot,u}$, where the ratio of total pressure at the target and at the equatorial plane is $e(T_e + T_i)n_e(1 + M^2)$, with the plasma flow Mach number M equal to 1 at the target for the the basic form of the Bohm–Chodura sheath condition. The value of p_{drop} for the large R_t varies from 0.5 (actual outer baffle) to 0.15 (longer outer baffle), from 0.7 to 0.29 for the extreme R_t and $p_{drop} \sim 1$ for the small R_t case, meaning no pressure drop.

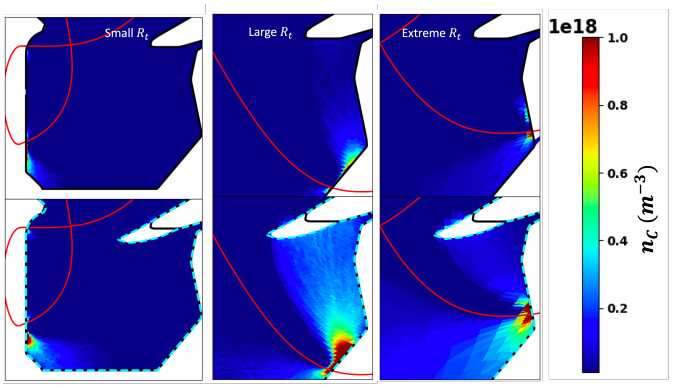

Figure 12: 2D divertor color plot of total carbon density C with the actual outer baffle (top row) and longer outer baffle (lower row). For the large and extreme R_t there is shown only the outer leg and strike point, where most the changes appear.

The simple TPM [12], without correction for power loss and momentum-pressure loss, cannot reproduce such effects and this disagreement can be also observed in fig. 15, where there is a scan in $n_{e,separatrix}$ of peak of J_{sat}, $T_{e,t}$ and target parallel heat flux $q_{\parallel,peak}$, comparing the actual outer baffle, fig. 15 (A), and the longer one, fig. 15 (B). The $J_{sat,peak}$ loses the quadratic dependence (expected from the simple TPM) on $n_{e,sep}$ with both outer baffles when $T_{e,peak}$ drops in the range of $10 - 5eV$, values at which the volumetric power and momentum-pressure loss start to be important on the ionization. The large and the extreme R_t with the longer outer baffle achieve the maximum value of $J_{sat,peak}$ at lower density, thanks to a more closed diver-

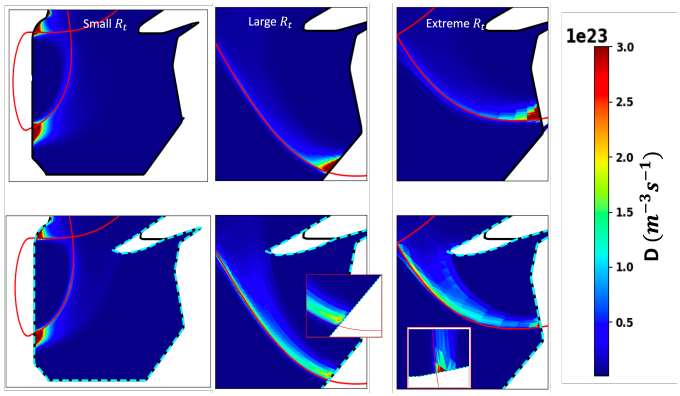

Figure 13: 2D divertor color plot of total ionization source with the actual outer baffle (top row) and longer outer baffle (lower row). For the large and extreme R_t there is shown only the outer leg and strike point, where most the changes appear.

tor, and start to reducing togheter with the $T_{e,t}$. The extreme R_t case shows the best performance in term of $q_{\parallel,target}$ peak drop with both types of the outer baffles for the higher R_t effect. The difference at the target between large R_t and extreme R_t, in particular the lower temperature for large R_t than the extreme R_t could be related to the different β and this will investigated in the future trying to find a way to fix a constant angle beta for all the three cases.

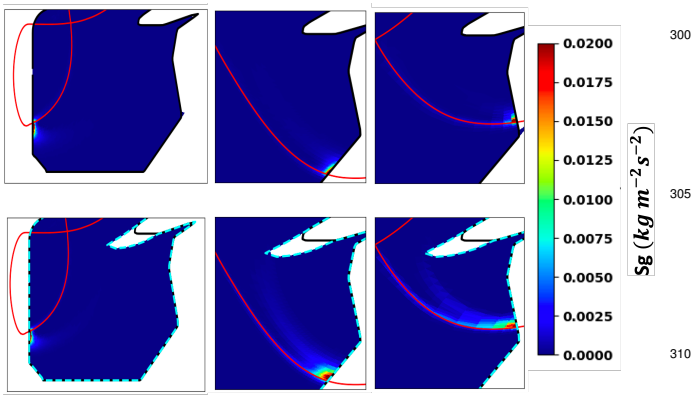

Figure 14: 2D divertor color plot of total momentum source with the actual outer baffle (top row) and longer outer baffle (lower row). For the large and extreme R_t there is shown only the outer leg and strike point, where most the changes appear.

.

5. Summary and conclusions

This work illustrates the impact of total flux expansion on divertor target profiles and on plasma detachment. 2D transport simulations with SolEdge2D-EIRENE reveal that density and temperature for increasing R_t do not change as TPM predictions partially because the neutral deuterium and carbon particles are not confined in the divertor region as well as the small R_t case, screening the beneficial effect of super-X at larger R_t. The extension outer baffle length needs to be changed to more closely

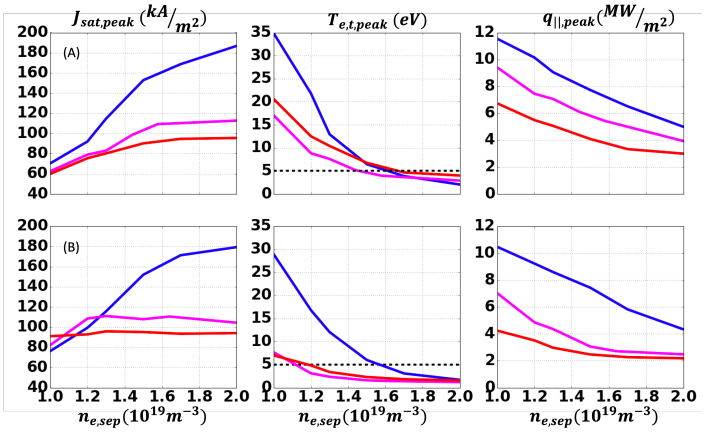

Figure 15: density evolution J_{sat}, $T_{e,target}$ and $q_{\parallel,peak}$ for the actual outer baffle (row A) and the longer one (row B)

retrieve beneficial effects of the Super-X, increasing the compression factor of large and extreme R_t above the small R_t value, reducing the neutral particle flux in the main chamber coming from the LFS. The variation in the compression factor is negligible for small case, because the neutrals are already well confined. The divertor region shows a consequent drop of 50% in electron temperature for the higher R_t cases, but the particles flux does not increase as we expected. This is related to the power and momentum losses. The first one is related to the rising of neutral deuterium and carbon compression factor with the larger outer baffle and the consequent increasing of total radiation. The second one is related to the friction forces between neutral and plasma particles and charge-exchange reactions that reducing the total target pressure compared with the equatorial one. The SOLEDGE2D simulations show also that particles flux start to not follow the simple TPM predictions at early density with the longer outer baffle compared with the experimental cases, anticipating the detachment onset. The large R_t case illustrated that with a longer outer baffle to improve the compression factor and same *beta* angle of small R_t is possible to have an high reduction of temperature and an early detachment onset. This motivate the necessity to improve the existed baffle in TCV machine to study the super-X. The extreme R_t shows a similar effect but it has apparently a worst result on target than the large R_t. This is caused by other effects, like the different *beta* angle to the wall. The future work will investigated the differences between large and extreme R_t. The extreme R_t, even if with smaller β angle compared to the other two has the best performance in term of heat and particle flux drop in front of the target. In this work we do not consider either the drifts or the neutral-neutral collisions. They could have a big impact on particle transport and change part of the SOLEDGE2D preliminary description. In future these aspect need to be investigated.

6. Acknowledgements

This work has been carried out within the framework of the EUROfusion Consortium, funded by the European Union via the Euratom Research and Training Programme (Grant Agreement No 101052200 — EUROfusion). Views and opinions expressed are however those of the author(s) only and do not necessarily reflect those of the European Union or the European Commission. Neither the European Union nor the European Commission can be held responsible for them. This work was supported in part by the Swiss National Science Foundation.

Bibliography

[1] European research roadmap to the realisation of fusion energy, tech. rep.
[2] Physics of ultimate detachment of a tokamak divertor plasma, Journal of Plasma Physics 83.
[3] T. W. Petrie, et al, Effect of changes in separatrix magnetic geometry on divertor behaviour in diii-d, Nucl. Fusion 53 (2013).
[4] C. Theiler, et all., Results from recent detachment experiments in alternative divertor configurations on tcv, Nucl. Fusion 57 (2017).
[5] A. Fill, et al, Separating the roles of magnetic topology and neutral trapping in modifying the detachment threshold for tcv, Plasma Phys. Control. Fusion 62 (2020).
[6] C. Theiler, et all, Advances in understanding power exhaust physics with the new, baffled tcv divertor, AIEA Fusion Energy Conf., 2020.
[7] H. Reimerdes, et al., Overview of the tcv tokamak experimental programme, Nuclear Fusion 62 (2022).
[8] H. Bufferand, et all, "soledge2d–eirene,", Nuclear materials and energy 12 852–857.
[9] J. Bohdansky, "an analytical formula and important parameters for low-energy ion sputtering", Journal of Applied Physics 51 (1980) 2861.
[10] D. Galassi, at all., "numerical investigation of optimal divertor gas baffle closure on tcv", Plasma Phys. Control. Fusion 62 (2020).
[11] Wensing, et all., Solps-iter validation with tcv l-mode discharges, Physics of Plasmas 28 (2021).
[12] H. P. Summers, Atomic data and analysis structure user manual, JET joint undertaking report (1994).
[13] P. C. Stangeby, The plasma boundary of magnetic fusion devices.